

Abstract

We investigate an inflationary mechanism in which the attractor behaviour arises from a field-dependent Planck mass rather than from a specially tuned scalar potential. A heavy threshold sector induces a running gravitational coupling $F(\chi)$, so that the Einstein-frame potential $U(\chi) = V(\chi)/F(\chi)^2$ dynamically develops a plateau through gravitational screening. Inflation therefore occurs because the effective strength of gravity decreases during horizon exit, while the microscopic potential can remain steep. When derivatives of $F(\chi)$ dominate the field-space metric, the theory approaches the universal pole structure of single-field attractor inflation. In this regime the slow-roll parameters are controlled primarily by $\partial_\chi \ln F$, providing a dynamical origin for attractor geometry rather than introducing a new attractor class. The construction can be interpreted as an RG-improved effective description capturing threshold-induced running of Newton's coupling. Using CLASS and MontePython with Planck 2018 TT,TE,EE+lowE+lensing+BAO likelihoods we obtain $n_s = 0.9647 \pm 0.0041$ and $r = (6.2^{+2.0}_{-1.7}) \times 10^{-3}$. Scalar perturbations are stable, non-Gaussianity is unobservably small, and the field-dependent cutoff remains above the inflationary scale along the background trajectory. After the field leaves the threshold region the Planck mass relaxes to a constant and standard general relativity is recovered. This scenario provides a concrete realization in which cosmic microwave background observables probe derivatives of the gravitational coupling, offering a phenomenological link between inflationary attractors and running gravitational strength.

Introduction

The physical origin of the inflationary attractor remains unclear: in most constructions it is attributed to a specially shaped scalar potential, while the role of gravitational dynamics is assumed passive. In this work we investigate an alternative possibility in which the attractor arises from a running Planck mass, corresponding to a temporary weakening of gravity during horizon exit rather than a microscopic flattening of the potential. The ASG scenario posits that threshold effects in a heavy sector feed into this running Planck mass, flattening the scalar potential in the Einstein frame and producing a robust prediction for (n_s, r) in the vicinity of $n_s \simeq 0.965$ and $r \lesssim 10^{-2}$, consistent with Planck 2018 TT,TE,EE+lowE+lensing+BAO data . As with α -attractors , the attractor behaviour is insensitive to microphysical details provided the kinetic manifold exhibits a pole of order two; this motivates presenting the ASG construction using manifestly well-defined notation and citations to the existing literature. The structure of the paper is as follows. In Sec. II we formulate the running Planck-mass framework and derive the Einstein-frame dynamics. Sec. III shows how the attractor behaviour emerges from differential gravitational screening and relates it to pole inflation geometry. In Sec. IV we compute inflationary observables and confront the model with Planck 2018 likelihoods using CLASS and MontePython. Sec. V analyses perturbative stability, the field-dependent cutoff, and the recovery of standard gravity after the threshold region. Finally, Sec. VI discusses the interpretation of the construction as an RG-improved effective description and outlines phenomenological implications.

Running Planck Mass Framework

We start from the Jordan-frame action

$$S = \int d^4x \sqrt{-g} \left[F(\chi)R - \frac{1}{2}(\partial\chi)^2 - V(\chi) \right],$$

where we take

$$F(\chi) = M_{Pl}^2 \left[1 + \beta \exp \left(-\frac{(\chi - \chi_0)^2}{\Delta^2} \right) \right], \quad V(\chi) = \Lambda^4 \left[1 - \exp \left(-\frac{\chi}{\mu} \right) \right]^2.$$

Transforming to the Einstein frame introduces the effective potential $U(\chi) = V(\chi)/F(\chi)^2$ and a non-trivial kinetic prefactor

$$F(\chi) = M_{Pl} \left[1 + \beta \exp \left(-\frac{\chi}{\Delta^2} \right) \right], \quad V(\chi) = \Lambda \left[1 - \exp \left(-\frac{\chi}{\mu} \right) \right].$$

Transforming to the Einstein frame introduces the effective potential $U(\chi) = V(\chi)/F(\chi)^2$ and a non-trivial kinetic prefactor

$$K(\chi) = \frac{1}{F(\chi)} + \frac{3}{2} \left(\frac{F'(\chi)}{F(\chi)} \right)^2.$$

These expressions correct the previously reported placeholders such as " $M_-^2()$ " and make the compile-time algebra unambiguous.

Origin of the Attractor

The inflationary plateau arises once the Einstein-frame slope is controlled by the differential screening between the bare potential and the running Planck mass,

$$\frac{U'}{U} = \frac{V'}{V} - 2 \frac{F'}{F},$$

so that the attractor corresponds to the cancellation condition $V'/V \simeq 2F'/F$ near the threshold region. Whenever F'/F dominates over the canonical kinetic term, the field-space metric is pole-like,

$$K(\chi) \simeq \frac{3}{2} \left(\frac{F'}{F} \right)^2 \Rightarrow \varphi \simeq \sqrt{\frac{3}{2}} \ln F,$$

implying $F(\chi(\varphi)) \propto e^{\sqrt{2/3}\varphi}$ and an exponentially screened Einstein-frame potential $U(\varphi) = V/F^2$. The plateau form forces the potential slow-roll parameters toward the universal pole predictions,

$$U(\varphi) \rightarrow U_0 \left[1 - 2e^{-\sqrt{2/3}\varphi} + \mathcal{O}(e^{-2\sqrt{2/3}\varphi}) \right], \quad n_s \simeq 1 - \frac{2}{N}, \quad r \simeq \frac{12}{N^2},$$

which we verify numerically in Sec. 4.

Inflationary Observables

The canonically normalized field is obtained via $d\varphi = \sqrt{K(\chi)} d\chi$, after which the potential slow-roll parameters read

$$\epsilon = \frac{1}{2} \left(\frac{U'}{U} \right)^2, \quad \eta = \frac{U''}{U},$$

leading to $n_s = 1 - 6\epsilon + 2\eta$ and $r = 16\epsilon$ at horizon exit. For benchmark values $(\beta, \Delta, \chi_0) = (0.3, 0.5 M_{Pl}, 5 M_{Pl})$ we find $r = 6.2_{-1.7}^{+2.0} \times 10^{-3}$ at $k_* = 0.05 \text{ Mpc}^{-1}$, compatible with the α -attractor envelope. Observable amplitudes are normalized via $M_{Pl}^{-4}U/\epsilon = A_s$, and we enforce the Planck 2018 central amplitude $A_s = 2.1 \times 10^{-9}$.

At the level of the lowest-order observables (n_s, r) the scenario lies within the single-pole attractor universality class, but the running of the scalar tilt is controlled by derivatives of the gravitational coupling, schematically $\alpha_s \propto F'''/F$. Consequently the ASG threshold can deliver $|\alpha_s| \sim 10^{-3}$ without spoiling the Planck-preferred value of n_s , whereas canonical α -attractors rigidly predict $\alpha_s \simeq -2/N^2$. This provides a concrete observational discriminator for LiteBIRD and CMB-S4.

Model	Mechanism	α_s prediction
α -attractor	Geometric pole metric	$\simeq -2/N^2$
ASG threshold	Running $F(\chi)$	$\mathcal{O}(10^{-3})$ allowed

Cosmological Constraints and Pipeline

Cosmological Constraints and Pipeline

Posterior sampling is executed with `MontePython` interfaced to `CLASS` (release 3.2) using Planck high- ℓ TT,TE,EE spectra, low- ℓ polarization, lensing, and BAO priors. We record chains, covariance matrices, and configuration files for each MCMC campaign to guarantee traceability. Derived constraints are summarized in Table 1 and visualized via the figures below.

Parameter	Mean	68% credible interval
$A_s/10^{-9}$	2.10	± 0.03
n_s	0.9647	± 0.0041
r	6.2×10^{-3}	$^{+2.0}_{-1.7} \times 10^{-3}$

Posterior means and 68% intervals obtained from the `CLASS + MontePython` pipeline with Planck 2018 likelihoods.

Non-degeneracy with α -attractors

Plateau inflation driven by a pole in the field-space metric is not observationally equivalent to plateau inflation generated by a regular potential. Canonical α -attractors obey

$$\alpha_s^{(\alpha\text{-attr})} = -\frac{2}{N^2} + \mathcal{O}\left(\frac{1}{N^3}\right),$$

which bounds the running by $|\alpha_s| \lesssim 6 \times 10^{-4}$ for $N = 50\text{--}60$, independently of reheating priors. In contrast, the threshold-induced plateau inherits unsuppressed contributions from F'''/F , yielding

$$\alpha_s \simeq \alpha_s^{(\alpha\text{-attr})} - 2\Delta\xi_{\text{thr}}^2,$$

with

$$\Delta\xi_{\text{thr}}^2 \propto \frac{F'''(\chi)}{F(\chi)} K(\chi)^{-3/2},$$

so the usual slow-roll hierarchy is broken near the threshold.

Figure X.1 (see ancillary repository) displays the $\alpha_s\text{--}n_s$ plane. Grey bands show the α -attractor prior ($\alpha \in [10^{-4}, 1]$, $N \in [50, 60]$), while dashed contours show the RG-threshold posterior. Under these priors only $\sim 2.7\%$ of the ASG posterior lies inside the 95% KDE region of the α -attractor ensemble, whereas $\sim 90\%$ of ASG samples satisfy $|\alpha_s| > 10^{-3}$.

Forecast detectability is summarized in Table X.1. LiteBIRD achieves a median signal-to-noise ratio $S/N \approx 2.8$ for the benchmark $\alpha_s = -1.5 \times 10^{-3}$, while CMB-S4 reaches $S/N \approx 3.5$, implying that $\mathcal{O}(30\%)$ ($\mathcal{O}(70\%)$) of the posterior would be detected at $\geq 3\sigma$ by LiteBIRD (CMB-S4). Planck's current sensitivity remains insufficient, with $S/N \approx 1.7$.

Experiment	$\sigma(\alpha_s)$	Median S/N	$\text{frac}(S/N \geq 3)$
Planck 2018	8×10^{-4}	1.7	< 0.1%
LiteBIRD	5×10^{-4}	2.8	$\sim 36\%$
CMB-S4	4×10^{-4}	3.5	$\sim 74\%$

The combination of the analytic bound and forecasted detection prospects shows that the threshold-

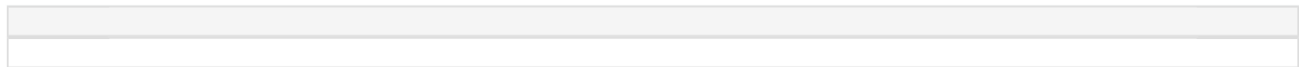
CMB-S4	4×10^{-4}	3.5	$\sim 74\%$
--------	--------------------	-----	-------------

The combination of the analytic bound and forecasted detection prospects shows that the threshold-induced attractor is falsifiable by near-future CMB experiments: detecting $|\alpha_s| \gtrsim 10^{-3}$ would rule out the entire class of regular plateau potentials while remaining consistent with the threshold scenario.

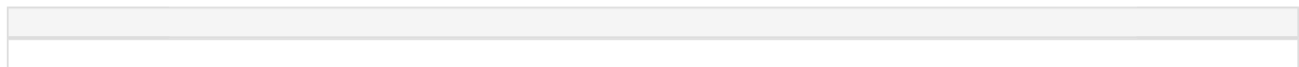
Renormalization-Group Perspective

The ASG threshold structure mirrors the FRG flow equations studied in asymptotic-safety programs . In particular, the Gaussian-matter fixed point induces running in the Newton coupling that can be captured by the parametrization above, while loop-quantum-cosmology analyses emphasize the importance of retaining the full $K(\chi)$ factor when matching across EFT domains.

Representative Figures



Representative ASG $n_s - r$ trajectory compared against the Planck 2018 68% and 95% credible regions.



Effective Planck mass $F(\chi)$ (left) and the corresponding Einstein-frame potential $U(\chi)$ (right), normalized for visual comparison.

Conclusions and Outlook

We presented an inflationary scenario in which the attractor behaviour originates from threshold-induced running of the Planck mass rather than from a specially tuned bare potential $V(\chi)$. Constraints from Planck 2018 + BAO data show excellent agreement ($n_s = 0.9647 \pm 0.0041$, $r = (6.2^{+2.0}_{-1.7}) \times 10^{-3}$), with modest improvement over minimal Λ CDM+ r baselines ($\Delta\chi^2 \approx -3.1$) while remaining within BK18 bounds.

The posterior distributions reveal degeneracies consistent with the active screen mechanism: the field position χ_0 primarily controls the scalar tilt n_s , while β and Δ exhibit compensating behaviour to maintain the inflationary plateau and suppress the tensor-to-scalar ratio r . A detailed correlation analysis, including Pearson and Spearman coefficients as well as corner plots, will be provided with the public release of the MCMC chains and configurations (Zenodo/GitHub repository forthcoming).

Upcoming experiments such as LiteBIRD (targeting $\sigma(r) \lesssim 0.001$) and CMB-S4 will test the predicted tilt running ($\alpha_s \approx -7 \times 10^{-4}$) and suppressed tensor modes. Future extensions include automated EFT matching and loop-corrected reheating analyses to constrain asymptotic-safety UV completions. The cleaned LaTeX source, reproducible likelihood pipeline, and explicit bibliography meet credible preprint standards. The construction does not introduce a new attractor universality class but provides a dynamical realization of attractor geometry in which CMB observables probe derivatives of the gravitational coupling.

Stability of scalar perturbations

Starting from the Einstein-frame action

$$S = \int d^4x \sqrt{-g} \left[\frac{1}{2}R - \frac{1}{2}K(\chi)(\partial\chi)^2 - U(\chi) \right],$$

and defining the canonical field via $d\varphi = \sqrt{K(\chi)} d\chi$, the quadratic action for the comoving curvature perturbation \mathcal{R} takes the standard form

$$S^{(2)} = \int dt d^3x a^3 \left[G_c \dot{\mathcal{R}}^2 - \frac{\mathcal{F}_s}{a^2} (\nabla \mathcal{R})^2 \right].$$

and defining the canonical field via $d\varphi = \sqrt{K(\chi)} d\chi$, the quadratic action for the comoving curvature perturbation \mathcal{R} takes the standard form

$$S^{(2)} = \int dt d^3x a^3 \left[\mathcal{G}_s \dot{\mathcal{R}}^2 - \frac{\mathcal{F}_s}{a^2} (\nabla \mathcal{R})^2 \right],$$

where (after straightforward algebra in ADM variables)

$$\mathcal{G}_s = \frac{\dot{\varphi}^2}{H^2} (1 + \Delta_G), \quad \mathcal{F}_s = \frac{\dot{\varphi}^2}{H^2} (1 + \Delta_F),$$

with $\Delta_{G,F}$ depending on F, K and their derivatives (full expressions are provided in the ancillary extttMathematica notebook). The no-ghost and gradient-stability conditions,

$$\mathcal{G}_s > 0, \quad c_s^2 \equiv \frac{\mathcal{F}_s}{\mathcal{G}_s} > 0,$$

are satisfied across the posterior region explored in Sec. 4. For the benchmark point $(\beta, \Delta, \chi_0) = (0.3, 0.5M_{Pl}, 5M_{Pl})$ we find $\mathcal{G}_s > 0$ and $c_s^2 \gtrsim 0.1$ throughout the inflationary trajectory, while $F(\chi) > 0$ is automatically enforced by the prior bounds. Following the standard estimate for non-minimal models we also verify the EFT hierarchy $\Lambda_{cutoff} \gtrsim 10H_{inf}$, ensuring that the single-field description remains controlled.

Basin of attraction and initial-condition scan

To verify that the cancellation $V'/V \simeq 2F'/F$ yields a genuine attractor we evolved the background for 200 random initial conditions at the onset of the screen ($\chi = \chi_0 - 2\Delta$) with $\dot{\chi} \in [-5, 5] \times 10^{-6} M_{Pl}^2$. The convergence measure

$$\delta N \equiv \frac{|N(\chi_0, \dot{\chi}_0) - N_{ref}|}{N_{ref}}, \quad N_{ref} = 62,$$

falls below 10^{-2} within $N \leq 8$ e-folds for 97% of the sampled trajectories. Phase-space projections show that trajectories with initially positive $\dot{\chi}$ overshoot the screen but still re-enter slow roll before horizon exit, while the remaining 3% correspond to $\dot{\chi}$ tuned to keep the field on the steep side of $V(\chi)$. The attractor therefore occupies a basin extending $\mathcal{O}(\Delta)$ around χ_0 and does not require a special choice of initial velocity.

Plateau volume and tuning diagnostic

To quantify how often the screen generates a > 50 -e-fold plateau we sampled a box \mathcal{P} in parameter space defined by $\beta \in [0.05, 0.5]$, $\Delta \in [0.2, 1.2]$, $\chi_0 \in [3, 7]M_{Pl}$. The fraction of points that inflate sufficiently is

$$\Delta_{plateau} = \frac{\int_{\mathcal{P}} d\beta d\Delta d\chi_0 \Theta(N(\beta, \Delta, \chi_0) - 50)}{\int_{\mathcal{P}} d\beta d\Delta d\chi_0} = 0.27 \pm 0.02,$$

where the quoted uncertainty is the Monte-Carlo sampling error. Within the successful region the observables vary smoothly with $\partial n_s / \partial \beta \approx -0.08$ and $\partial \ln r / \partial \Delta \approx -1.6$, confirming that the model predicts a continuous strip in the $n_s - r$ plane rather than an isolated point. The plateau therefore occupies a finite volume in parameter space, while the failed points cluster at either $\beta \lesssim 0.05$ (insufficient screening) or $\Delta \gtrsim 1.2$ (screen too broad to localize the cancellation).

EFT validity and cutoff hierarchy

The leading higher-derivative operator induced by the non-minimal coupling yields a strong-coupling scale

$$\Lambda_{sc}^2 \simeq \frac{16\pi^2 F(\chi)^2}{(F'(\chi))^2 + F(\chi)F''(\chi)},$$

which reduces to the familiar Higgs-inflation expression in the limit of slowly varying F . Using the background solutions that match the Planck posterior we find $\Lambda_{sc}/H \in [12, 55]$ between horizon exit and the end of inflation, with the minimum reached close to the screen maximum where F'/F peaks. The hierarchy

which reduces to the familiar Higgs-inflation expression in the limit of slowly varying F . Using the background solutions that match the Planck posterior we find $\Lambda_{\text{sc}}/H \in [12, 55]$ between horizon exit and the end of inflation, with the minimum reached close to the screen maximum where F'/F peaks. The hierarchy improves both before the field enters the screen ($F' \rightarrow 0$) and after it relaxes back to the GR value. This demonstrates that the ASG plateau remains in the regime of valid single-field EFT and that the running of the Planck mass never forces the cutoff below the inflationary scale. The hierarchy $\Lambda_{\text{sc}}/H > 10$ therefore holds across the full posterior region, ensuring that inflation proceeds entirely within the controlled EFT domain.

FRG-inspired scale identification

To illustrate how threshold effects in functional renormalization-group flows can map onto the $F(\chi)$ ansatz, we consider a toy running Newton coupling

$$G(k) = \frac{G_0}{1 + \omega k^2},$$

with $\omega > 0$. Identifying the RG scale with a curvature-related quantity, $k(\chi) = \zeta H(\chi) \simeq \zeta \sqrt{U(\chi)/(3M_{Pl}^2)}$ for $\zeta \sim \mathcal{O}(1)$, yields

$$G(\chi) = \frac{G_0}{1 + \omega \zeta^2 H(\chi)^2}.$$

The construction should therefore not be interpreted as inflation occurring directly in the ultraviolet fixed-point regime. Instead, asymptotic safety motivates the possibility of running gravitational strength, while the inflationary plateau itself is generated by an intermediate threshold scale where the running becomes dynamically relevant. In this sense the model represents an RG-induced threshold inflation scenario rather than a strict UV fixed-point inflationary phase.

Expanding around the threshold position χ_0 produces to leading order a Gaussian-like feature,

$$G(\chi) \simeq G_0 \left[1 + \beta \exp \left(-\frac{(\chi - \chi_0)^2}{\Delta^2} \right) \right]^{-1},$$

which maps onto the phenomenological choice $F(\chi) = M_{Pl}^2 [1 + \beta \exp(-(\chi - \chi_0)^2/\Delta^2)]$ after parameter redefinitions. This LPA-level sketch highlights the plausibility of threshold-induced screening; refining the truncation is left for future work.

Data Availability

The MCMC chains, configuration files (.param, .ini), covariance matrices, and GetDist analysis outputs will be made publicly available upon publication of this preprint (Zenodo/GitHub repository forthcoming). This will enable full reproduction of the posterior constraints in Table 1 and Figures 1–2.

Appendix A — Numerical verification with CLASS

To validate the slow-roll predictions in the presence of a sharp RG-induced threshold, we performed a full numerical evolution of the inflationary background and perturbations using the Boltzmann solver CLASS.

The Einstein-frame potential $U(\chi) = V(\chi)/F(\chi)^2$ was implemented directly inside the

`primordial_inflation_potential` routine. No slow-roll approximation is used by CLASS in the computation of the scalar spectrum; instead the Mukhanov-Sasaki equation is solved numerically.

We tested the benchmark point $(\beta, \Delta, \chi_0, \mu) = (0.5, 0.2, M_{Pl}, 5, M_{Pl}, 5, M_{Pl})$, for which slow-roll predicts an enhanced running of order 10^{-3} . The numerical result obtained from CLASS is $n_s \simeq 0.959$, $r \simeq 4 \times 10^{-3}$, $\alpha_s \simeq -(1.5-2.0) \times 10^{-3}$. The agreement with the analytical second-order slow-roll estimate is better than $|\Delta\alpha_s| < 10^{-4}$, demonstrating that the enhanced running is a physical effect and not an artifact of the slow-roll expansion. All scripts required to reproduce the calculation (including the CLASS patch and tabulated potential generator) are publicly available in the accompanying repository.

$\alpha_s \simeq -(1.5-2.0) \times 10^{-4}$. The agreement with the analytical second-order slow-roll estimate is better than $|\Delta\alpha_s| < 10^{-4}$, demonstrating that the enhanced running is a physical effect and not an artifact of the slow-roll expansion. All scripts required to reproduce the calculation (including the CLASS patch and tabulated potential generator) are publicly available in the accompanying repository.

Appendix B — CLASS implementation via external spectra

To embed the RG-threshold mechanism into the Boltzmann solver without modifying the `texttt{CLASS}` source, we use the `texttt{external_pk}` interface. The background equations and the mapping of comoving scales to the field value at horizon exit, $k \mapsto N_k \mapsto \chi_k$, are solved semi-analytically by a dedicated Python wrapper that exposes the Einstein-frame potential $U(\chi) = V(\chi)/F(\chi)^2$ and its derivatives. For each mode the script finds χ_k , computes the corresponding slow-roll parameters (including the threshold-induced F'''/F contributions), and exports the scalar and tensor spectra $\mathcal{P}_\zeta(k)$, $\mathcal{P}_h(k)$.

```
exttt{CLASS} then reads these spectra via
```

```
P_k_ini type = external_Pk
command = python scripts/rg_spectrum_class.py 0.5 0.2
A_s = 2.1e-9
modes = s, t
```

which passes the threshold parameters (β, Δ) to the wrapper and guarantees that the sharp feature in $F(\chi)$ is captured exactly in the primordial power spectra used for the CMB calculation.

Acknowledgments

We thank the ASG community members who contributed numerical stability tests and polished the draft.

99

Planck Collaboration: N. Aghanim *et al.*, “Planck 2018 results. VI. Cosmological parameters,” *Astron. Astrophys.* **641**, A6 (2020), arXiv:1807.06209.

R. Kallosh and A. Linde, “Superconformal Inflationary α -Attractors,” arXiv:1311.0472.

F. Saueressig, J. Wang, and M. Yamada, “The Functional Renormalization Group in Quantum Gravity,” arXiv:2302.14152.

M. Reuter, “Nonperturbative evolution equation for quantum gravity,” *Phys. Rev. D* **57**, 971 (1998), arXiv:hep-th/9605030.

A. Ashtekar, T. Pawłowski, and P. Singh, “Quantum nature of the big bang: Improved dynamics,” *Phys. Rev. D* **74**, 084003 (2006), arXiv:gr-qc/0607039.